Nanoindentation tests of heavy-ion-irradiated Au foams—molecular dynamics simulation

Carlos J. Ruestes, Christian Anders, Eduardo M. Bringa, and Herbert M. Urbassek

Citation: Journal of Applied Physics **123**, 225903 (2018); doi: 10.1063/1.5027191
View online: https://doi.org/10.1063/1.5027191
View Table of Contents: http://aip.scitation.org/toc/jap/123/22
Published by the American Institute of Physics

Nanoindentation tests of heavy-ion-irradiated Au foams—molecular dynamics simulation

Carlos J. Ruestes,[1] Christian Anders,[2] Eduardo M. Bringa,[3] and Herbert M. Urbassek[2,a)]
[1]*CONICET and Facultad de Ciencias Exactas y Naturales, Universidad Nacional de Cuyo, Mendoza 5500, Argentina*
[2]*Physics Department and Research Center OPTIMAS, University Kaiserslautern, Erwin-Schrödinger-Straße, D-67663 Kaiserslautern, Germany*
[3]*CONICET and Facultad de Ingeniería, Universidad de Mendoza, Mendoza 5500, Argentina*

(Received 28 February 2018; accepted 28 May 2018; published online 14 June 2018)

Irradiation by light ions may change the mechanical properties of nanofoams. Using molecular-dynamics simulation, we study the effect of irradiating a Au foam (porosity, 50%, and ligament diameter, 3 nm) with heavy ions: here, 10 keV Au ions up to a dose of 4×10^{16} m^{-2}. We demonstrate that in consequence, the ligament morphology changes in the irradiated region, caused by local melting. The changes in mechanical properties are monitored by simulated nanoindentation tests. We find that the foam hardness is only around 1/3 of the hardness of a bulk Au crystal. Irradiation increases the hardness of the foam by around 10% in the central irradiated area. The plastic zone extends to only 1.5 a_c, where a_c denotes the contact radius; this value is unchanged under irradiation. The hardness increase after irradiation is attributed to two concurring effects. To begin with, irradiation induces melting and annealing of the ligaments, leading to their coarsening and alleviating surface stress, which in turn increases the dislocation nucleation threshold. In addition, irradiation introduces a stacking fault forest that acts as an obstacle to dislocation motion. *Published by AIP Publishing.* https://doi.org/10.1063/1.5027191

I. INTRODUCTION

Metallic foams have acquired interest due to their light weight and the high stiffness of their structural elements, and the recent availability of nanofoams[1] offers new potential. In the case of Au, the mechanical properties of nanofoams have been explored both experimentally and using molecular dynamics (MD) simulation. On the experimental side, the techniques of uniaxial compression and nanoindentation were employed,[2–6] and it could be demonstrated that, at the nanoscale, foam strength is governed by ligament size, in addition to relative density. MD simulations studied the behavior of Au nanofoams in the same loading scenarios; the focus of these studies lays on the behavior of dislocations and stacking faults (SFs) under applied stresses and also the tension-compression asymmetry and the so-called anomalous compliance of these foams in the elastic regime.[7–11]

Radiation-induced hardening in metals has been extensively studied for decades using experiments, modeling, and simulation,[12–14] but several issues still require a better understanding of technological applications.[15] In particular, the response of nanofoams to ion irradiation is relevant for potential uses of these materials as radiation shields, for instance, in a space environment where weight concerns are relevant.[16] It was found that such materials exhibit a considerable radiation resistance which is caused by the high surface-to-volume ratio that assists the annealing of radiation-induced defects.[17–20] In these studies, often the irradiation by light ions (He and Ne) is used, which results in dilute collision cascades with recoil energies of a few or a few ten keV. The damage induced by the heavier recoils may result in quite different damage patterns since they lead to localized energy deposition (the so-called spikes[21,22]), which may even melt up the foam locally.

Intense irradiation will induce defects in the foam and hence change its mechanical properties. The behavior of Au nanofoams in particular was studied in some detail using both experiments and MD simulations. Bringa *et al.*[18] studied nanoporous Au foams under irradiation and concluded that foams can be tailored to become radiation tolerant. A similar conclusion was drawn by Fu *et al.*[19] who provided further insights into the deformation mechanisms due to irradiation, in an interplay of ligament coarsening, formation of stacking-fault-tetrahedra (SFTs), and twinning. In later experiments, nanoindentation was used to measure the effect of irradiation on nanoporous gold, finding that hardness increases after irradiation.[23] Avoiding the complexity of foams, several MD studies focused on exploring the effects of ion irradiation of single Au nanowires as a simple model for a ligament in a nanofoam.[24–26] In particular, the work of Figueroa *et al.*[25] identified the generation of dislocations and twins in the sample as well of SFTs and demonstrated an increase in flow stress in the nanowire, in agreement with experiments.[23]

In the present paper, we study the irradiation of a Au nanofoam with 10 keV Au ions and the subsequent changes in mechanical hardness using MD simulation. Such energetic Au ions may appear in the course of any higher-energy irradiation as recoils (primary knock-on atoms) and hence constitute a typical damage pattern. We test for the resulting changes in the foam morphology, the induced damage, and the response to nanoindentation.

a)Electronic mail: urbassek@rhrk.uni-kl.de. URL: http://www.physik.uni-kl.de/urbassek/

II. METHOD

A. Irradiation method

An extended gold foam target was prepared from a foam template generated by a phase-field model simulating the spinodal decomposition of a binary alloy.[27,28] The foam has a porosity of $p = 0.5$ and an average ligament size of 3 nm. The initially prepared structure was repeated in lateral directions 3 times and in the vertical direction twice in order to set up a target of sufficient size for irradiation and subsequent hardness analysis. The target has an extension of approximately $55 \times 55 \times 37\,\mathrm{nm}^3$ containing around 3.5×10^6 Au atoms. The target is single-crystalline with a (100) surface.

Impact simulations are performed using the MD simulation package LAMMPS[29] with an NVE ensemble and the velocity Verlet integrator. The interaction between the gold atoms was modeled by an embedded-atom-model potential developed by Colla and Ubrassek,[30] which reproduces the melting temperature for Au, $T_m = 1338\,\mathrm{K}$,[31,32] and has an interaction cutoff radius of $r_c = 6.2$ Å. In order to model high-energy collisions, this potential is splined to the Ziegler-Biersack-Littmark potential.[33] Electronic stopping in the target was disregarded since its effects can be considered minor at these impact energies. Within a distance of one lattice constant from the lower and lateral boundaries, atom motion is damped using the recipe of Beeler,[34] which applies a velocity-proportional friction force $F_r = -Rv$. The damping constant R is adjusted to achieve the critical damping of the atom oscillations; in our case, this results in $R = 0.6614$ eV ps Å^{-2}.

The Au foam target is irradiated by 10 consecutive impacts of 10 keV Au ions. Ions impact randomly in a central area of $15 \times 15\,\mathrm{nm}^2$ around the center in order to prevent the interaction of the collision cascades with the boundaries. The ion impact is not normal to the surface in order to avoid channeling along the [100] direction; rather, each ion impacts at 7° to the normal and random azimuth. The irradiation dose in this central area thus amounts to roughly $4 \times 10^{16}\,\mathrm{m}^{-2}$.

Because of the high impact energy, an adaptive time step was used, with a value between 0.01 fs and 1 fs. 10^5 MD steps (roughly 98 ps) were sufficient to simulate the impacts and the ensuing energy dissipation to the surroundings. The temperature in the damaged surface ligaments was then below the melting point of Au. After each impact, the target was relaxed by applying a friction force with a damping constant of $R = 0.1$ eV ps Å^{-2} for all atoms for 10 000 MD steps.

We determined the "irradiation-affected zone" by determining all atoms that ever were above melting temperature. This zone has a surface area of $30 \times 30\,\mathrm{nm}^2$ and extends to a depth of 25 nm. Of course, some recoils of the collision cascades may reach out even further, but they will only lead to point defects, not to structural changes in the ligaments.

Figure 1 shows a cross-sectional cut through the foam before and after the impact. The local structure is illustrated with the help of the centro-symmetry parameter.[35] It is seen that already the virgin foam contained SFs caused by the production process.[27,28] Irradiation has a profound effect on the foam structure in the irradiation-affected zone. The high energy deposition of the Au projectiles partly melts the structure such that ligaments change the shape and ligament joints may break up or form newly. A few changes in the morphology can also be observed slightly outside this zone and indicate that besides melting, also the mechanical stresses occurring under bombardment may induce changes in the adjacent regions not immediately affected by irradiation. In addition, in the zone, new SFs and dislocations are generated; quantitatively, the total length of dislocations showed an increase in roughly 20%.

Figure 2 shows how the surface topography changed due to the irradiation. In the center of the impact area, ligaments have been heavily deformed and the surface has become depressed. In order to quantify the effect of irradiation on the sample, we employed the recently developed AQUAMI software[36] to measure the average ligament diameter change as a function of the depth in the irradiation-affected zone. Our analysis shows that irradiation caused the average ligament diameter to increase by around 10 percent at depths between 2 and 10 nm below the surface.

B. Indentation method

In order to explore the changes in the mechanical response due to irradiation, nanoindentation simulations are

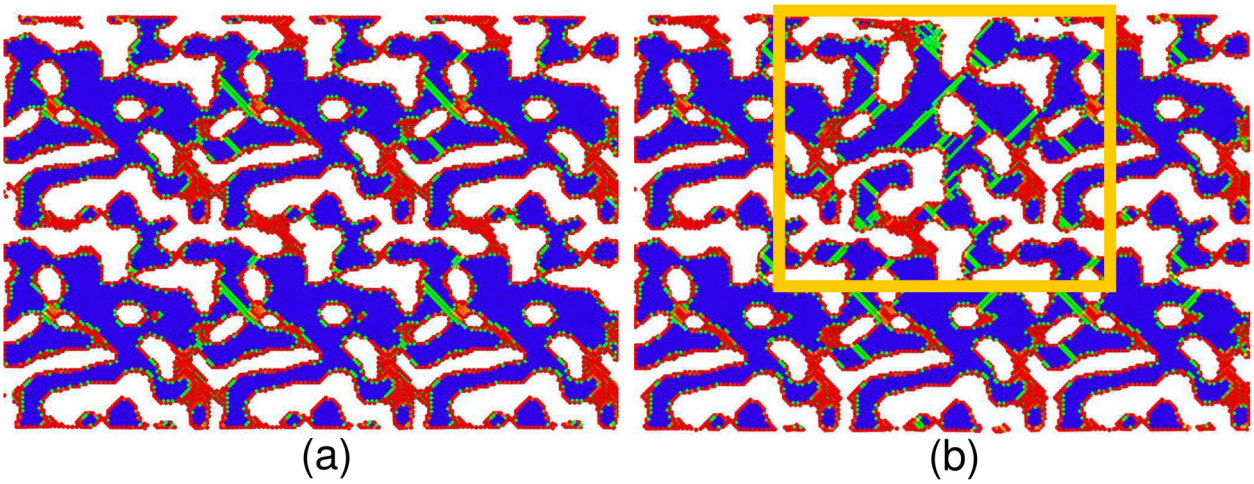

FIG. 1. Cross-sectional cut (0.5 nm thick) through the foam before (a) and after (b) irradiation by 10 ions. The irradiation-affected zone is marked by a rectangle. Atoms are colored according to their local structure using the centro-symmetry parameter. Red: surface, blue: fcc, and green: hcp.

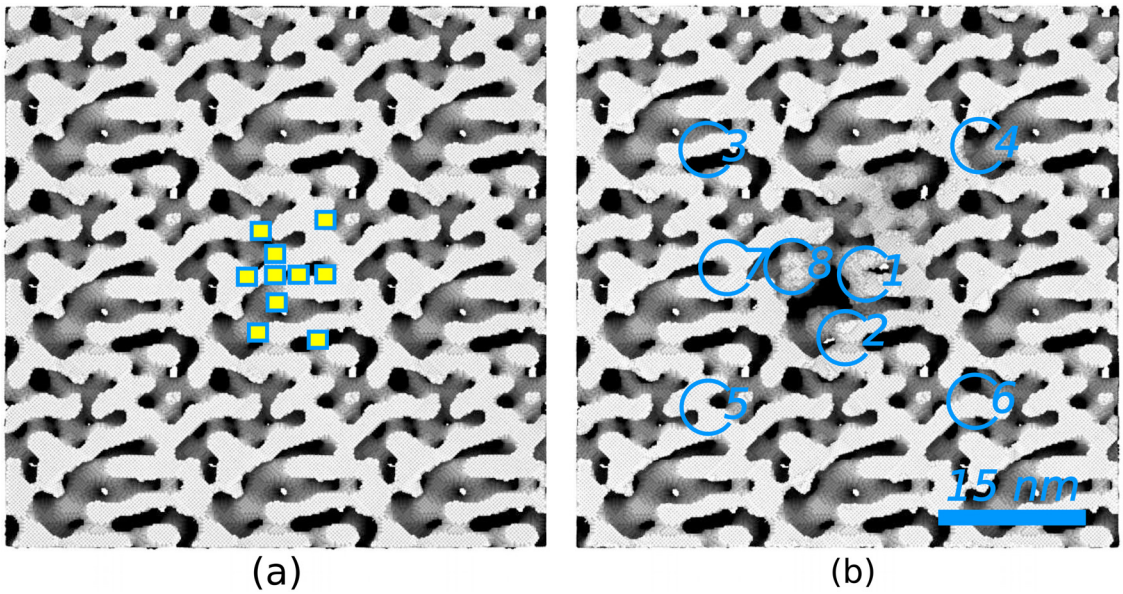

FIG. 2. Top view of (a) the non-irradiated foam (ion impact positions are marked) and (b) the irradiated sample (positions of indent points are marked and numbered). The gray-scale indicates the height of the surface structures.

performed following the procedure described below, both for the original and for the irradiated foam.

We fix two atom layers at the bottom and at the side faces of the foam in order to suppress any rigid-body movement of the foam. The next four layers at the bottom and the sides are thermostatted to keep the temperature below 1 K in the simulation in order to rule out thermally activated processes. Before performing the nanoindentation simulations, the foams are relaxed until all stress components have reached values $<10^{-5}$ GPa.[37] The indentation velocity is chosen as 10 m/s. This velocity, although high compared with the experimental indentation, is within the range typically used in MD studies and amounts to less than 1 percent of the longitudinal wave velocity of gold.

The tip has a spherical shape with a radius of $R = 15$ nm. It interacts in a purely repulsive way with the substrate atoms according to the law[35]

$$V(r) = \begin{cases} k(R-r)^3, & r < R, \\ 0, & r \geq R. \end{cases} \quad (1)$$

Here, r is the distance of a substrate atom to the center of the indenter and $k = 10\,\text{eV/Å}^3$ (Refs. 35 and 38) is a constant. For the indenter model chosen, there are no tangential forces, akin to a Hertzian indenter.

Figure 2 visualizes the 8 indent positions used. The positions will be described as P1–P8 in the following: Positions 1, 2, and 8 are central in the irradiated area, while 3 to 6 are at the periphery, and P7 is intermediate. The indentation depth amounts to 6 nm in all cases such that the contact radius of the indenter is 12 nm. In consequence, the indenter tip probes the response of several ligaments simultaneously; such a behavior corresponds to the situation encountered in the experiment. We checked that for all indenter positions, the indent pit does not interfere with the boundary of the simulation volume.

The MD simulations are performed using the open-source LAMMPS code[29] with a constant time step of 2 fs. The software tool OVITO[39] is used for the visualization of the results; DXA[40] is employed for the analysis of the dislocations generated.

III. RESULTS

A. Contact pressures

The hardness of the material is defined as the contact pressure in the plastic regime, which is established once the critical indentation for nucleating dislocations has been exceeded. In order to determine the attained contact pressures, the evolution of load has to be related to the contact area. For that purpose, we will consider the projection of the convex contact surface onto the initial surface plane by using an atomistic approach; the contact area A^{atom} is the sum of the projected areas of all atoms i that are in contact with the indenter[38]

$$A^{\text{atom}} = \pi\beta^2 \sum_{i\,\epsilon\,\text{contact}} \cos\,\alpha_i. \quad (2)$$

Here, β is an atom radius and α_i is the angle formed by the indentation direction and the vector joining the center of the indenter with atom i. For Au, we choose $\beta = 1.44$ Å.

Figure 3 presents the contact pressure considering the contact area through Eq. (2). For comparison purposes, Fig. 3(a) includes the response of a bulk Au single crystal in the same orientation (100). Note that the foams all agree in their elastic part, but the load drop caused by the nucleation of dislocations occurs considerably earlier in the foams than in the bulk material. This is plausible since the large amount of the surface available in the foam alleviates dislocation nucleation.

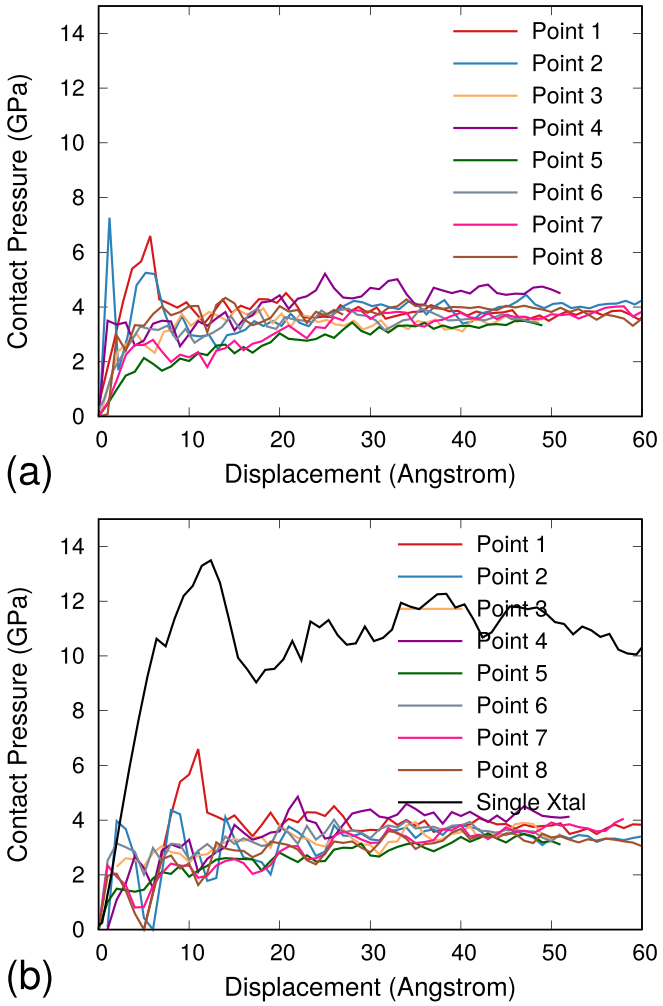

FIG. 3. Evolution of the contact pressure with the penetration depth for the (a) original and (b) the irradiated foam. For comparison, the simulation result for a single-crystalline Au specimen has been added to (a).

We analyzed in detail the hardness data of Fig. 3. Concentrating on the data for a displacement of >3 nm—where the contact pressure has assumed stable values—we evaluate the average contact pressure, which is identical to the foam hardness H, and assemble the values in Table I; there, in addition, the fluctuations of the data are quantified. We observe an increase in the hardness after irradiation by 6%. Most interesting is the variation of the hardness changes with the irradiation point. For the central points P1, P2, P7, and P8, the average increase amounts to 10%, with a maximum of 18.5% for P8. On the other hand, for the peripheral indents, P3–P6, the increase amounts to only 3.4%. We conclude that—despite the large fluctuations inherent in hardness evaluations in a foam material—the trend of increased hardness in the center of the irradiated area is clear.

Such an increase is in agreement with previous studies of the effect of irradiation on nanofoams, which reported a ∼15% increase under irradiation.[23]

The Au hardness derived here is in the range of 10–12 GPa for the single crystal. The hardness of the nanofoam is considerably smaller, in line with the easier dislocation nucleation. These values are of the order of magnitude

TABLE I. Hardness evaluated at the indent positions P1–8 for the (a) original and the (b) irradiated foam. Data for the average hardness H, the standard deviation, and error, as well as the maximum and minimum values, have been evaluated during the last 3 nm of penetration. All data are given in the units of GPa.

(a)

Point	H	Std. Dev.	Std. Err.	Max	Min
P1	3.76	0.23	0.038	4.06	3.06
P2	3.44	0.18	0.035	3.79	3.09
P3	3.48	0.26	0.056	3.92	3.09
P4	4.20	0.17	0.039	4.59	3.94
P5	3.15	0.22	0.050	3.49	2.67
P6	3.64	0.18	0.037	3.97	3.23
P7	3.54	0.25	0.049	4.05	3.16
P8	3.28	0.19	0.035	3.68	2.83
Average	3.56	0.21	0.042	3.94	3.13

(b)

Point	H	Std. Dev.	Std. Err.	Max	Min
P1	3.77	0.14	0.025	4.06	3.49
P2	4.00	0.20	0.032	4.45	3.39
P3	3.52	0.23	0.036	3.89	3.11
P4	4.58	0.24	0.057	5.01	4.08
P5	3.28	0.09	0.022	3.43	3.06
P6	3.59	0.19	0.041	3.95	3.15
P7	3.70	0.16	0.026	4.02	3.72
P8	3.89	0.16	0.030	4.28	3.57
Average	3.79	0.17	0.033	4.14	3.44

of the yield strength of Au nanowires under tension[41,42] and will be discussed further in Sec. III D below.

B. Dislocations

It is known from experiments that the main defects involved in the plastic deformation of nanoporous gold under tension[7] and compression[9,10] are Lomer-Cottrell locks and Shockley partials.[43]

We display in Fig. 4 the dislocations found after indentation into the original and the irradiated foams. Indeed, we identify a majority of Shockley partials with Burgers vector $\boldsymbol{b} = \frac{1}{6}[\bar{1}\bar{2}1]$. In addition, Lomer-Cottrell dislocation locks can be spotted, together with a few full dislocations $\left(\boldsymbol{b} = \frac{1}{2}[110]\right)$. In small numbers, also Hirth sessile dislocations $\left(\boldsymbol{b} = \frac{1}{3}[001]\right)$ and Frank dislocations $\left(\boldsymbol{b} = \frac{1}{3}[111]\right)$ were found. Further classes of dislocations were also found; a detailed analysis revealed that they are mainly double stair-rod dislocations with $\boldsymbol{b} = \frac{1}{6}[022]$.[9,24] We conclude that a rich array of dislocations are formed by indentation into the nanofoam; the differences between the original and the irradiated foam could not be observed.

Figure 5 displays how the total length of Shockley partial dislocations evolved during indentation, together with the number of SFs. Indentation point P2 has been analyzed as a representative example both for the original and for the irradiated foam.

Figure 5(a) demonstrates that the total length of the dislocation lines of Shockley partials has been doubled by the

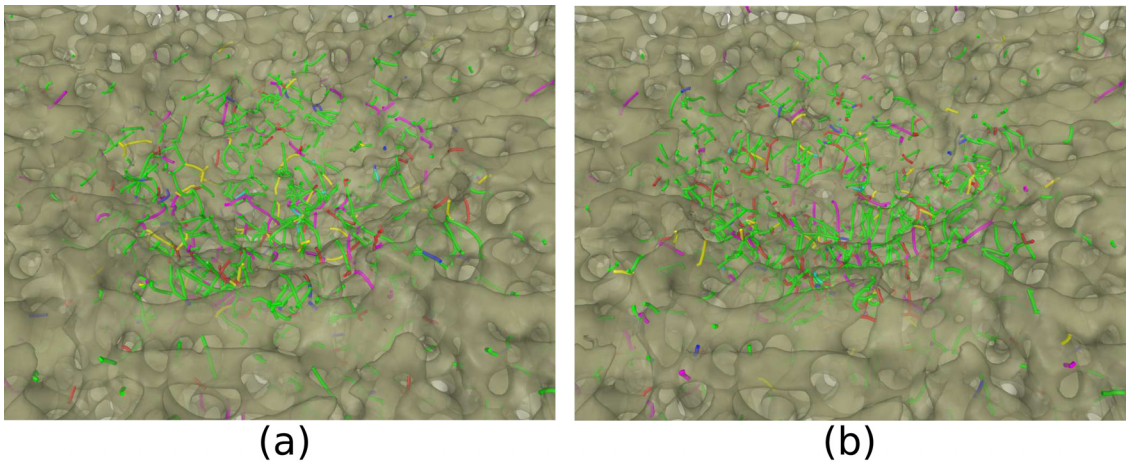

FIG. 4. Top view of the dislocation structure obtained after indenting the (a) original and the (b) irradiated foam at P1 to a depth of 6 nm. Green: Shockley partials, blue: full dislocations, pink: stair-rod dislocations, yellow: Hirth partials, cyan: Frank partials, and red: other dislocations, including double stair-rod dislocations.

indentation process. Assuming a line length of an average Shockley partial of 2 nm—equivalent to the ligament diameter—the original foam contained around 200 dislocations, and this number has been approximately doubled by indentation. Note that irradiation does not generate Shockley partials.

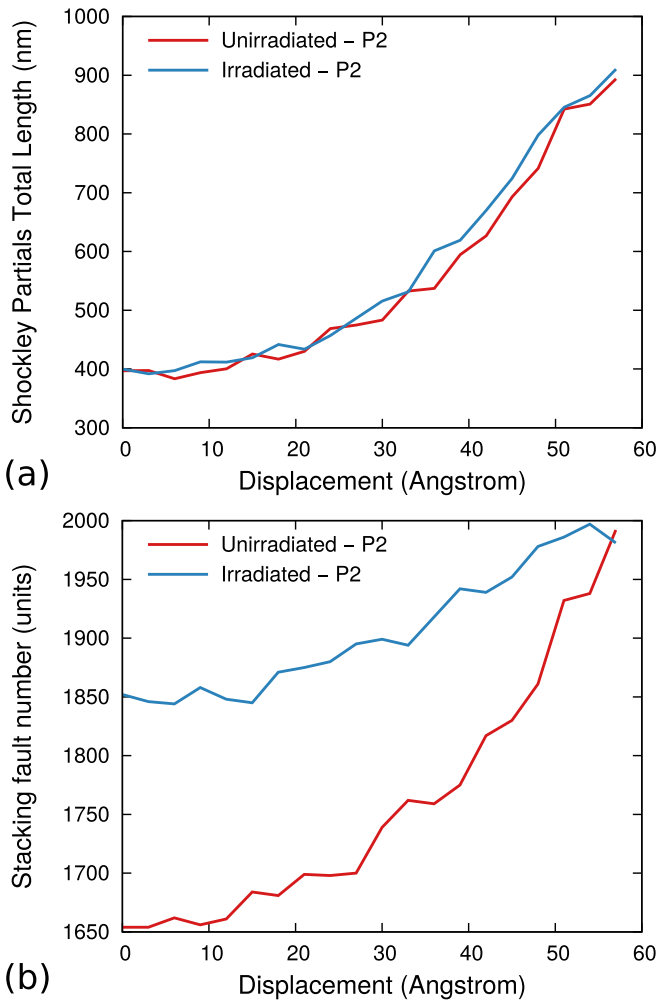

FIG. 5. Evolution of the total dislocation length of Shockley partials (a) and of intrinsic SFs (b) with the penetration depth for indentation in P2 for the original and the irradiated foams.

The number of SFs present in the original and in the irradiated foams and their evolution during indentation are displayed in Fig. 5(b). While irradiation does not introduce Shockley partials to the foam, it induces a considerable number of SFs. In addition, indentation generates SFs more abundantly in the unirradiated foam. This feature is consistent with the idea that unirradiated ligament surfaces are rough, while spike melting made them smoother; unirradiated ligaments are thus more prone to dislocation nucleation than ligaments relaxed by irradiation, which would nucleate less partials from a smoother surface. This feature is consistent with the conclusions by Rabkin and Srolovitz for dislocation nucleation in gold nanopillars with different surfaces.[44]

The relatively larger number of SFs in the irradiated foam contributes to hardening as there are more defects that might be impeding dislocation movement. We note that our analysis also showed that irradiation also increased the initial number of stair-rod dislocations, which are sessile dislocations that can further contribute to the increase in hardness. In the unirradiated foam, dislocations nucleate, travel, and annihilate on the opposite ligament surface, leaving SFs as a residue. While this is consistent with the concept of dislocation starvation,[45] the dislocation count reveals that the overall scenario is that of dislocation accumulation. In the irradiated foam, Shockley partials increase with a similar rate as in the original foam, while SFs now increase less steeply. This feature suggests that dislocations again nucleates and propagates but are not sufficient to reach a surface for annihilation due to the pre-existing SF forest, which plays the role of obstacles, preventing their movement; hence, the generation of SFs is lower, contributing to the hardening.

A dislocation accumulation scenario has already been observed in nanoporous gold, both in experiments[46,47] and in MD studies.[10,48]

In order to characterize the plastic activity under nanoindentation, Fig. 6 displays the atomic shear strain that resulted in the original and in the irradiated foam after full indentation to 6 nm on P1. High strains occur at the surface, immediately below the indenter. Note, however, that below the surface, strain is localized in planes; these are the glide planes of dislocations, which are here visualized by the strain. These glide

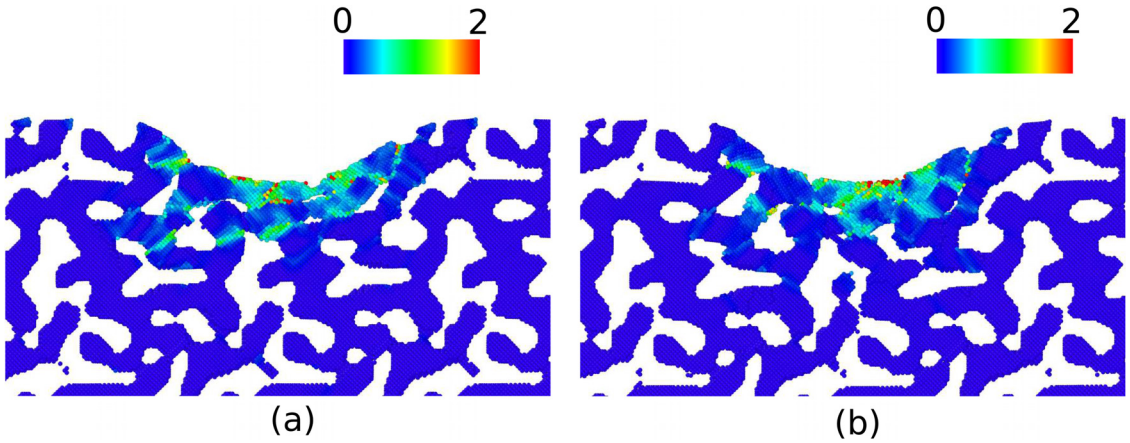

FIG. 6. Cross-sectional cut (0.5 nm thick) through the (a) original and the (b) irradiated foam after indenting at P1 to a depth of 6 nm. Atoms are colored according to atomic strain [see the color bar].

planes give rise to the SFs that will be visualized in Fig. 7. Shear maximizes at the filament nodes, which are particularly subject to failure by dislocation activity.

Interestingly, the strain as an indicator of dislocation activity appears to be more localized towards the surface in the irradiated foam, and the signatures of large strains in the ligaments situated farther away from the indenter has decreased. This indicates that the irradiation-induced melting has alleviated the surface stress in the sample. The initial strains far away from the indenter [Fig. 6(a)] do not show up after irradiation [Fig. 6(b)]. The plastic zone in both cases is small, as ligaments constrain dislocation motion locally, in line with recent studies.[48,49]

C. Plastic zone

The size of the plastic zone generated by indentation is of considerable importance for the understanding of nanoindentation.[50] Since in this respect we found no difference between the original and the irradiated foams, we shall discuss the plastic zone only for the original foam. In previous contributions,[51,52] the plastic zone generated by nanoindentation was described as a hemisphere centered on the indent point. The radius of the hemisphere, R_{pl}, was determined as the largest distance of a dislocation line to the indent point. In this work, we extended this definition to include the region where dislocations and SFs were introduced by indentation since these denote the primary sort of defects created. The size factor f of the plastic zone is introduced as the ratio of R_{pl} to the radius of the contact area, a_c,

$$f = \frac{R_{\mathrm{pl}}}{a_c}. \tag{3}$$

Figure 7 compares the results of a common-neighbor analysis[53] for the original foam before indentation and for a 6 nm penetration on Point 1. It can be seen qualitatively that planar defects appear to be concentrated in the vicinity of the filament junctions. The planar defects mostly show up as SFs; a few dislocations can be recognized in the right hand side of panel Fig. 7(b), for instance, as white dots in the end of some short red segments. The SFs are created so abundantly since the majority of dislocations glided through the ligaments and annihilated at a surface, leaving behind the SFs, depicted in red. From a quantitative evaluation of these data, we obtain a size factor of $f = 1.5$. This is significantly lower than the values for bulk fcc metals reported by Gao *et al.*[51] which are in the range of $f = 3$–4, suggesting that np-foams are effective

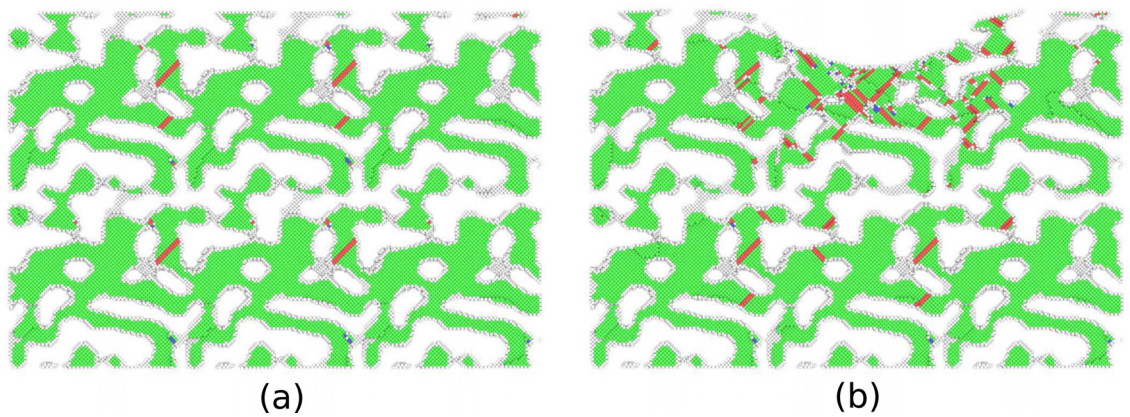

FIG. 7. Cross-sectional cut (0.5 nm thick) through the original foam before (a) and after (b) indentation on P1; the penetration depth is 6 nm. Note that this cut is perpendicular to that of Fig. 6. Atoms are colored according to their local structure using common-neighbor analysis. Green: fcc, red: hcp, indicating SFs, blue: bcc, and white: other.

materials for the confinement of plasticity in the cases of dynamic indentation.

Finally, Fig. 8 displays the typical imprint produced by indentation. In contrast to the indentation of bulk samples, no hillocks are found around the imprint and no pileup. However, the compaction of the foam can be appreciated inside the imprint, in agreement with the experimental literature.[49,54] Furthermore, the foam does not exhibit significant lateral expansion during the penetration of the indenter, as the pores simply collapse under the tip and accommodate the imposed displacement.

D. Discussion

Figueroa *et al.*[25] showed that keV self-irradiation of a large (25 nm diameter) Au nanowire produces vacancies and SFs, which serve as dislocation nucleation sites, because the energy required for nucleation is smaller at such defects than the energy required for dislocation nucleation at free surfaces. As a result, the yield strength under tension or compression decreases. However, the scenario in our case appears to be different. The irradiation-induced thermal spikes result in annealing of the ligaments. Due to melting, Au tries to minimize its surface area; hence, ligaments coarsen and their surfaces are modified and relaxed, which increases the stresses required for dislocation nucleation. It is known that surface modifications can alter the surface stress, delaying dislocation nucleation, as shown by Rabkin and Srolovitz.[44] These authors showed that minor changes in the surface structure, such as the removal of loosely bound atoms, lead to an increase in the stress required for dislocation nucleation and slip, or in other words, that rough surfaces are more prone to generate dislocations than smooth surfaces. Melting produces smooth surfaces and hence less dislocation activity, in line with our findings. In addition, Yang *et al.*[55] studied the effect of irradiation on the mechanical behavior of pre-strained Cu nanowires, suggesting that keV-level ion irradiation can be used to tune the mechanical properties of nanowires, such as to eliminate the residual stresses. This points to the important role of surface stresses since surface tension can significantly influence the mechanical properties of nanoporous gold, as shown by Farkas *et al.*[8] and Mameka *et al.*[56]

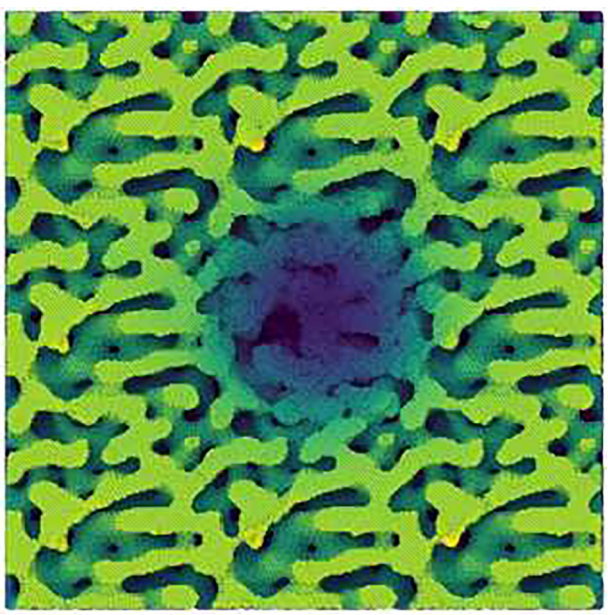

FIG. 8. Top view of the imprint (penetration depth, 6 nm) on the irradiated sample for indentation on P1. The color indicates the height above the original surface.

Nanoindentation is a technique that does not test the mechanical properties of individual ligaments but rather senses the mechanical response of an ensemble of ligaments and pores, and as a result, discrepancies often arise between yield-strength measurements through tensile testing and those inferred from nanoindentation testing, as pointed out by Leitner *et al.*[57] Briot and Balk[49] performed focused ion beam characterization of deformation resulting from the nanoindentation of nanoporous gold, concluding that a factor analogous to a constraint factor (C) should be applied for a proper correlation of yield strength (σ) with hardness (H)

$$H \approx C\sigma. \tag{4}$$

The determination of a proper hardness-to-yield-strength ratio, C, is not simple since it varies with the indenter type and mechanical properties of the material, such as yield strength, Young's modulus, hardening index, and Poisson's ratio.[58–61]

For sharp indenters probing bulk solids, in which volume is conserved during plastic deformation, the constraint factor is in the range of 2.5–3.0, depending on friction and indenter tip,[62] and it also depends on further properties of the material such as the Poisson ratio[61] and the yield-strength-to-elastic-modulus ratio.[63] For simplicity, we will consider $H \approx 3\sigma$, rendering a yield strength for the pristine single crystal in the range of 3.3–4 GPa, which is remarkably close to the theoretical critical shear strength, $\tau_{th} \approx G/(2\pi)$.

For metallic foams exhibiting non-volume-conserving plasticity, the constraint factor is approximately in the range of 1.0 to $(1+2p)$ with the porosity p according to Ashby *et al.*,[64] that is, between 1.0 and 2.0 for our np sample with $p = 0.5$. Mangipudi *et al.*[65] reported a hardness-to-yield stress ratio of 2.7 for nanoporous gold, slightly above the value of 2.65 used by Briot and Balk[49,66] to reconcile their hardness and tensile test measurements. If we use the upper bound value of C (2.7) so that each calculation of the foam yield strength derived from Eq. (4) results in a lower bound, then the foam yield strength obtained from the average contact pressure is in the range of 1.3–1.4 GPa, remarkably close to the yield strength of Au nanowires under tension.[41,42]

The difference between the hardness of a foam and a single crystal can thus be attributed to the fact the foam has plenty of potential dislocation sources at the surface of the ligaments.

IV. SUMMARY

Ion irradiation changes the mechanical properties of nanofoams. Using molecular-dynamics simulation, we study this effect by irradiating a Au foam (porosity, 50%; ligament diameter, 3 nm) with 10 keV Au ions up to a dose of 4×10^{16} m^{-2}. In consequence, the ligament morphology changes in the irradiated region, caused by local melting. The changes in

mechanical properties are monitored by simulated nanoindentation tests. We find that the foam hardness is only around 1/3 of the hardness of a bulk Au crystal. Irradiation increases the hardness of the foam by around 10% in the central irradiated area. The plastic zone extends to only $1.5a_c$, where a_c denotes the contact radius; this value is unchanged under irradiation, while dislocation activity after irradiation is more strongly localized under the indenter surface, indicating that the irradiation-induced melting has stabilized the ligaments.

The hardness increase after irradiation is attributed to two concurring effects. Irradiation induces melting and annealing of the ligaments, leading to their coarsening and alleviating surface stress, which in turn increases the dislocation nucleation threshold. In addition, irradiation introduces a stacking fault forest that acts as an obstacle to dislocation motion.

The irradiation-induced effects on mechanical properties are smaller than those observed in the previous work on 40–400 keV He or Ne irradiation,[23] in which lower-energy Au recoils are created. Our case of more energetic Au irradiation produces collision spikes, in which local melting leads to a partial self-annealing of the generated defects. In particular, the SFTs that were observed after light-ion irradiation were not produced in our case, and hence, no true obstacles to dislocation motion. However, it must be noted that our heavy-ion irradiation simulations do describe the effect of Au PKAs that arise during light-ion irradiation in experiments, and therefore, the hardness increase presented here can be favorably compared with the hardness increase reported by Caro *et al.*[23]

ACKNOWLEDGMENTS

H.M.U. acknowledges the support from the Deutsche Forschungsgemeinschaft via Sonderforschungsbereich 926. E.M.B. acknowledges the support from ANPCyT PICT-2014-0696 and SECTyP-UNCuyo. C.J.R. acknowledges the support from ANPCyT PICT-2015-0342 and SECTyP-UNCuyo and a donation from Nvidia Corporation. The irradiation simulations were performed at the High Performance Cluster Elwetritsch (RHRK, TU Kaiserslautern, Germany), while the indentation simulations were performed at TOKO Cluster (FCEN—UNCuyo, Mendoza, Argentina). The authors thank D. Farkas for providing the np-Au sample used in this study.

[1]B. C. Tappan, S. A. Steiner, and E. P. Luther, Angew. Chem. Int. Ed. **49**, 4544 (2010).
[2]C. Volkert, E. Lilleodden, D. Kramer, and J. Weissmüller, Appl. Phys. Lett. **89**, 061920 (2006).
[3]J. Biener, A. M. Hodge, J. R. Hayes, C. A. Volkert, L. A. Zepeda-Ruiz, A. V. Hamza, and F. F. Abraham, Nano Lett. **6**, 2379 (2006).
[4]A. Hodge, J. Biener, J. Hayes, P. Bythrow, C. Volkert, and A. Hamza, Acta Mater. **55**, 1343 (2007).
[5]Y. Sun, J. Ye, Z. Shan, A. M. Minor, and T. J. Balk, JOM **59**, 54 (2007).
[6]Y. Sun, J. Ye, A. M. Minor, and T. J. Balk, Microsc. Res. Tech. **72**, 232 (2009).
[7]X.-Y. Sun, G.-K. Xu, X. Li, X.-Q. Feng, and H. Gao, J. Appl. Phys. **113**, 023505 (2013).
[8]D. Farkas, A. Caro, E. Bringa, and D. Crowson, Acta Mater. **61**, 3249 (2013).
[9]C. J. Ruestes, D. Farkas, A. Caro, and E. M. Bringa, Acta Mater. **108**, 1 (2016).
[10]B.-N. D. Ngô, A. Stukowski, N. Mameka, J. Markmann, K. Albe, and J. Weissmüller, Acta Mater. **93**, 144 (2015).
[11]B.-N. Ngô, B. Roschning, K. Albe, J. Weissmüller, and J. Markmann, Scr. Mater. **130**, 74 (2017).
[12]T. D. de la Rubia, H. M. Zbib, T. A. Khraishi, B. D. Wirth, M. Victoria, and M. J. Caturla, Nature **406**, 871 (2000).
[13]M. Victoria, N. Baluc, C. Bailat, Y. Dai, M. Luppo, R. Schaublin, and B. Singh, J. Nucl. Mater. **276**, 114 (2000).
[14]J. Robach, I. Robertson, B. Wirth, and A. Arsenlis, Philos. Mag. **83**, 955 (2003).
[15]S. J. Zinkle and L. L. Snead, Annu. Rev. Mater. Res. **44**, 241 (2014).
[16]S. A. Thibeault, J. H. Kang, G. Sauti, C. Park, C. C. Fay, and G. C. King, MRS Bull. **40**, 836 (2015).
[17]J. F. Rodriguez-Nieva, E. M. Bringa, T. A. Cassidy, R. E. Johnson, A. Caro, M. Fama, M. J. Loeffler, R. A. Baragiola, and D. Farkas, Astrophys. J. Lett. **743**, L5 (2011).
[18]E. M. Bringa, J. D. Monk, A. Caro, A. Misra, L. Zepeda-Ruiz, M. Duchaineau, F. Abraham, M. Nastasi, S. T. Picraux, Y. Q. Wang *et al.*, Nano Lett. **12**, 3351 (2012).
[19]E. G. Fu, M. Caro, L. A. Zepeda-Ruiz, Y. Wang, K. Baldwin, E. Bringa, M. Nastasi, and A. Caro, Appl. Phys. Lett. **101**, 191607 (2012).
[20]J. F. Rodriguez-Nieva and E. M. Bringa, Nucl. Instrum. Methods B **304**, 23 (2013).
[21]P. Sigmund, Appl. Phys. Lett. **25**, 169 (1974); **27**, 52 (1975).
[22]T. J. Colla, R. Aderjan, R. Kissel, and H. M. Urbassek, Phys. Rev. B **62**, 8487 (2000).
[23]M. Caro, W. M. Mook, E. G. Fu, Y. Q. Wang, C. Sheehan, E. Martinez, J. K. Baldwin, and A. Caro, Appl. Phys. Lett. **104**, 233109 (2014).
[24]L. Zepeda-Ruiz, E. Martinez, M. Caro, E. Fu, and A. Caro, Appl. Phys. Lett. **103**, 031909 (2013).
[25]E. Figueroa, D. Tramontina, G. Gutierrez, and E. Bringa, J. Nucl. Mater. **467**, 677 (2015).
[26]C. Zhang, Y. Li, W. Zhou, L. Hu, and Z. Zeng, J. Nucl. Mater. **466**, 328 (2015).
[27]D. A. Crowson, D. Farkas, and S. G. Corcoran, Scr. Mater. **56**, 919 (2007).
[28]D. A. Crowson, D. Farkas, and S. G. Corcoran, Scr. Mater. **61**, 497 (2009).
[29]S. Plimpton, J. Comput. Phys. **117**, 1 (1995), see http://lammps.sandia.gov/.
[30]T. J. Colla and H. M. Urbassek, Nucl. Instrum. Methods B **164-165**, 687 (2000).
[31]S. Zimmermann and H. M. Urbassek, Nucl. Instrum. Methods B **228**, 75 (2005).
[32]S. Zimmermann and H. M. Urbassek, Nucl. Instrum. Methods B **255**, 208 (2007).
[33]J. F. Ziegler, J. P. Biersack, and U. Littmark, *The Stopping and Range of Ions in Solids* (Pergamon, New York, 1985).
[34]J. R. Beeler, Jr., *Radiation Effects Computer Experiments* (North-Holland, Amsterdam, 1983).
[35]C. L. Kelchner, S. J. Plimpton, and J. C. Hamilton, Phys. Rev. B **58**, 11085 (1998).
[36]J. Stuckner, K. Frei, I. McCue, M. J. Demkowicz, and M. Murayama, Comput. Mater. Sci. **139**, 320 (2017).
[37]G. Ziegenhain, H. M. Urbassek, and A. Hartmaier, J. Appl. Phys. **107**, 061807 (2010).
[38]G. Ziegenhain, A. Hartmaier, and H. M. Urbassek, J. Mech. Phys. Sol. **57**, 1514 (2009).
[39]A. Stukowski, Model. Simul. Mater. Sci. Eng. **18**, 015012 (2010).
[40]A. Stukowski and K. Albe, Model. Simul. Mater. Sci. Eng. **18**, 085001 (2010).
[41]B. Wu, A. Heidelberg, and J. J. Boland, Nat. Mater. **4**, 525 (2005).
[42]C. R. Weinberger and W. Cai, J. Mater. Chem. **22**, 3277 (2012).
[43]D. Hull and D. J. Bacon, *Introduction to Dislocations*, 3rd ed. (Pergamon Press, Oxford, 1984), Vol. 257.
[44]E. Rabkin and D. J. Srolovitz, Nano Lett. **7**, 101 (2007).
[45]J. R. Greer and W. D. Nix, Phys. Rev. B **73**, 245410 (2006).
[46]R. Dou and B. Derby, J. Mater. Res. **25**, 746 (2010).
[47]R. Dou and B. Derby, Philos. Mag. **91**, 1070 (2011).
[48]D. Farkas, J. Stuckner, R. Umbel, B. Kuhr, and M. J. Demkowicz, J. Mater. Res. **33**, 1382 (2018).
[49]N. J. Briot and T. J. Balk, MRS Commun. **8**, 132 (2018).
[50]K. Durst, B. Backes, and M. Göken, Scr. Mater. **52**, 1093 (2005).
[51]Y. Gao, C. J. Ruestes, D. R. Tramontina, and H. M. Urbassek, J. Mech. Phys. Sol. **75**, 58 (2015).
[52]I. Alabd Alhafez, C. J. Ruestes, Y. Gao, and H. M. Urbassek, Nanotechnology **27**, 045706 (2016).
[53]H. Tsuzuki, P. S. Branicio, and J. P. Rino, Comput. Phys. Commun. **177**, 518 (2007).

[54]J. Biener, A. M. Hodge, A. V. Hamza, L. M. Hsiung, and J. H. Satcher, Jr., J. Appl. Phys. **97**, 024301 (2005).
[55]Z. Yang, F. Jiao, Z. Lu, and Z. Wang, Sci. China Phys., Mech. Astron. **56**, 498 (2013).
[56]N. Mameka, J. Markmann, and J. Weissmüller, Nat. Commun. **8**, 1976 (2017).
[57]A. Leitner, V. Maier-Kiener, J. Jeong, M. Abad, P. Hosemann, S. Oh, and D. Kiener, Acta Mater. **121**, 104 (2016).
[58]M. Shaw and T. Sata, Int. J. Mech. Sci. **8**, 469 (1966).
[59]K. Johnson, J. Mech. Phys. Solids **18**, 115 (1970).
[60]A. Bhattacharya and W. Nix, Int. J. Solids Struct. **27**, 1047 (1991).
[61]A. C. Fischer-Cripps, *Introduction to Contact Mechanics* (Springer, 2000).
[62]M. C. Shaw and G. J. DeSalvo, Metallogr., Microstruct., Anal. **1**, 310 (2012).
[63]Y.-T. Cheng and C.-M. Cheng, J. Appl. Phys. **84**, 1284 (1998).
[64]M. F. Ashby, T. Evans, N. A. Fleck, J. Hutchinson, H. Wadley, and L. Gibson, *Metal Foams: A Design Guide* (Elsevier, 2000).
[65]K. Mangipudi, E. Epler, and C. Volkert, Scr. Mater. **146**, 150 (2018).
[66]N. J. Briot and T. J. Balk, Philos. Mag. **95**, 2955 (2015).